

This is the submitted version of the article:

López-Suárez, M.; Pruneda, M.; Abadal, G.; Rurali, R..
Piezoelectric monolayers as nonlinear energy harvesters.
Nanotechnology, (2014). . . : - .
10.1088/0957-4484/25/17/175401.

Available at:

<https://dx.doi.org/10.1088/0957-4484/25/17/175401>

See discussions, stats, and author profiles for this publication at: <https://www.researchgate.net/publication/261603394>

Piezoelectric monolayers as nonlinear energy harvesters

Article in *Nanotechnology* · April 2014

DOI: 10.1088/0957-4484/25/17/175401 · Source: PubMed

CITATIONS

16

READS

138

4 authors:



Miquel López-Suárez

Materials Science Institute of Barcelona

38 PUBLICATIONS 142 CITATIONS

[SEE PROFILE](#)



Miguel Pruneda

Catalan Institute of Nanoscience and Nanotechnology

79 PUBLICATIONS 1,951 CITATIONS

[SEE PROFILE](#)



Gabriel Abadal

Autonomous University of Barcelona

141 PUBLICATIONS 1,951 CITATIONS

[SEE PROFILE](#)



Riccardo Rurali

Materials Science Institute of Barcelona

170 PUBLICATIONS 3,786 CITATIONS

[SEE PROFILE](#)

Some of the authors of this publication are also working on these related projects:



Gas sensor [View project](#)



Energy Harvesting at micro and nanoscale [View project](#)

Non-linear energy harvesting in BN nanoribbons from molecular dynamics

Miquel López-Suárez

Department of Physics, University of Perugia, via A. Pascoli, 1, 06100 Perugia, Italy

Gabriel Abadal

*Departament d'Enginyeria Electrònica, Universitat Autònoma de Barcelona, 08193
Bellaterra, Barcelona, Spain*

Luca Gammaitoni

Department of Physics, University of Perugia, via A. Pascoli, 1, 06100 Perugia, Italy

Riccardo Rurali

*Institut de Ciència de Materials de Barcelona (ICMAB-CSIC), Campus de Bellaterra,
08193 Bellaterra (Barcelona), Spain*

Abstract

We present molecular dynamics calculations of a h -BN nanoribbon designed for vibrational energy harvesting. We calculate the piezoelectric voltage generated at the ends of the device as a function of time and for different level of an external compressive strain. Through the full atomistic description of the nanoribbon dynamics we demonstrate that driving the system into a non-linear dynamical regime greatly increase its harvesting efficiency.

Keywords: Energy harvesting, non-linear oscillators, boron nitride, molecular dynamics

Introduction

Energy harvesting from mechanical vibrations is commonly performed through oscillating mechanical structures, i.e. cantilevers, clamped-clamped beams, etc.

*Corresponding author

Recently, it has been shown that engineered non-linearities increase significantly the performances of these devices due to the broadening of the frequency response, a crucial advantage when it comes to harvest broad spectral densities such as those of ambient vibrations [? ?]. Additionally, shrinking the dimension of such structures results in an increment of the harvesting efficiency in terms of power density. This is easily seen by considering a piezoelectric linear oscillator, whose generated electric power is [?] $P_{rms} \sim m a_{rms}^2 f_r$, where m is the mass of the oscillator, a_{rms} is the root mean square acceleration of the external excitation, and f_r is the resonance frequency. Downscaling the device size by a factor $h < 1$, the output power at a given a_{rms} scales as h^2 , which means that the power density, P_{rms}/V , increases by a factor $1/h$.

In a previous work, we have reported the outstanding harvesting efficiency of a suspended *h*-BN nanoribbon [?]. A slight compressive axial strain is used to induce a buckling of the ribbon that, when it oscillates, behaves like a bistable device (see the sketch in Fig: ??a). The combination of the quasi-linear oscillations within each potential well with the low frequency swing from one well to the other provides the aforementioned spectral broadening and results in a harvested electrical power of 0.18 pW from a 5 pN vibration. The compressive strain is the only control parameter and is used to tune the dynamics of the system: a threshold strain is needed to induce the bistability, but a too large strain would trap the system in one of the two wells, preventing swings between the two wells.

In Ref. [?] the potential landscape was obtained through state-of-the-art, quantum calculations within density-functional theory (DFT) [?]. The price to pay for the great accuracy of those calculations was two-fold: (i) a simplified description of the dynamics of the system, which was reduced to the motion of a point-like particle with an effective mass and one single degree of freedom; (ii) the systems studied were smaller than nanoribbons experimentally fabricated and the presence of the ribbon edges was neglected.

The goal of this work is providing a much more realistic description of the system and its dynamical evolution in presence of ambient noise. We study

realistic 100 nm long and 7 nm wide *h*-BN nanoribbons and account for the individual dynamics of each of the ~ 28000 atoms of the system. We use an extensively tested classical interatomic potential to describe the interaction among the atoms. This allows us affording the computational cost of such large-scale system and studying its dynamical evolution for several nanoseconds.

Computational Methods

We study a 233×30 supercell of the rectangular 4-atom unit cell of 2D *h*-BN (Fig: ??b) that results in a $100.8 \text{ nm} \times 7.5 \text{ nm}$ armchair nanoribbon containing 27960 atoms. We perform molecular dynamics (MD) calculations within the NVT ensemble using the LAMMPS code [?] and a Langevin thermostat [?]. The system is initially thermalized at $T = 300 \text{ K}$ for 1 ns in order to equilibrate the structure. The same thermal bath is considered as the external vibration source, thus matching the strength of the external force to $F_{rms}^{ext} = \sqrt{4bk_bTf_r}$ —where b is the mechanical damping, k_b the Boltzmann constant, T the temperature, and f_r the resonance frequency— which is considered to be the minimum measurable force on a mechanical system [?]. After the equilibration, the dynamic simulation is carried out for 25 ns, while all atomic coordinates are monitored to obtain a full description of the system dynamics. This procedure is repeated for different compression values. The potential energy and the forces are accounted for with a a bond-order Tersoff potential as parameterized by Sevick *et al.* [?]. This potential gives an equilibrium lattice parameter for *h*-BN of 2.498 Å, in very good agreement with previous DFT reports [?]. We calculate the 2D polarization along the x -axis as [? ?]:

$$P_x^{2D} = \sum_i^N \frac{q_i x_i}{A} \quad (1)$$

where A is the area of the ribbon, q_i and x_i are the charge and x -coordinate of the i -th atom and the sum runs over all the N atoms. We use $2.7|e|$ and $-2.7|e|$ for B and N, respectively, values obtained by DFT calculation of bulk *h*-BN [?] and BN nanotubes [?]. The conventional polarization, as defined in

bulk materials, can be related to the 2D polarization as $P = P^{2D}t$, where t is an effective thickness of the h -BN sheet. We take $t = 3.5 \text{ \AA}$, the interlayer separation of multilayer bulk h -BN.

Results and discussion

Static Calculations

At first we calculated the elastic potential energy as a function of the amplitude of the oscillation in the simple case in which only the fundamental vibrational mode is excited. For this purpose, similarly to our previous works [? ?], for each value of the strain we generate several sinusoidal deformations of increasing amplitude, and we calculate the total energy and the polarization for each of these configurations. As the strain is applied, two symmetric potential wells develop, corresponding to the two equivalent buckled configurations that allow releasing most of the strain (see Fig. ??). When the compression increases the wells become deeper and their separation increases, making energetically more expensive to commute from well to the other, as shown in inset of Fig. ?. While the ribbon buckle under compression to allow the relaxation of the in-plane strain, ribbon stretching ($c > 0$) is directly translated into internal strain ($\epsilon_{int} = c$) and a change in the polarization, is observed.

These calculations are similar to those we reported previously and, while not adding new information, they demonstrate the capability of the Tersoff potential to describe the bistability of a h -BN nanoribbons under compression. This is an important point, because if the results obtained with the classical potential are in qualitative agreement with those obtained with more sophisticated –and computationally expensive– quantum mechanical methods, we can now tackle full atomistic MD simulations of a realistic nanoribbon.

As a further proof of the capabilities of the Tersoff potential to describe the buckling of the h -BN nanoribbon, we have performed a direct comparison with the potential landscapes obtained by DFT using the same structural model of Ref. [?] (2D h -BN without edges, $17 \text{ nm} \times 1 \text{ nm}$ supercell). The excellent

agreement between the two sets of calculations is shown in Fig. ?? for the case of the uncompressed ribbon (b) and a 2 % compression (c).

Dynamic Calculations

Using the setup described in the previous section, i.e. clamping the ends of the ribbon and applying different degrees of compression, we performed extensive molecular dynamics simulations in the NVT ensemble, with $T = 300$ K. In these simulations no assumption on the dynamics of the atoms or on the shape of the excited vibrational modes is made: after the system has been thermalized its dynamical evolution is observed and the position of the atoms of a central region of the ribbon is recorded [?]. Notice that within dynamical simulation using a Langevin thermostat, the polarization P_x^{2D} has two components: one as a consequence of the collective vibrational mode along z , and another due to thermal in-plane strains along x . The second term seems to dominate the voltage generation when considering $T = 300$ K, thus, in order to reduce its contribution, we have also performed MD simulations at $T = 0$ K, adding a stochastic external force, F_{ext} , parallel to z that acts on each atom of the system. The effective temperature, T_{eff} , is around 120 K ($F_{rms} = 510^{-3}$ eV/Å. These simulations allow isolating in a clearer way the gain of the compressed configuration.

The MD runs that we have performed nicely capture the bistability of the system when a moderate compressive strain is applied, but reveal a much more complex behavior in the transition from one well to the other, which is the key to the increased harvesting efficiency. Some representative snapshots of the dynamics of a nanoribbon with a compression of 1.5 % are shown in Fig. ?. While the fundamental mode, with a sinus like profile, is recognizable and corresponds to the system vibrating in one of the wells (Fig. ??a, c, and e), the first excited mode, with a node in the middle of the ribbon, often shows up (Fig. ??b). Noticeably, the transition between the two symmetric ground states of the potential energy is almost always mediated by such a mode, rather than going through the ideally flat configuration (the saddle point in Fig. ??a; flat

configurations of that kind are only seldom observed and typically look like the superposition/interference of several vibrational modes, Fig ??d).

In order to get a more quantitative insight on the dynamics we have studied the dependence of the root-mean-square of the out-of-plane displacement, $z_{r.m.s.}$, of the atoms as a function of the applied compression (see Fig. ??, left). When characterizing ambient vibration harvesting, $z_{r.m.s.}$ is a good indicator of the device performance, because the maximum generated electric power is obtained for compressions close to those that maximize it: roughly speaking, a higher oscillating amplitude generates higher strains in the piezoelectric transducing element, which increases the piezoelectric voltage $V_{r.m.s.}$. This holds, for instance, for energy harvesting devices with piezoelectric transducers working in the 31 mode [?]. Fig. ?? clearly illustrates the three dynamical regimes: (i) for low compression, $c \sim 0$ the ribbon exhibit a quasi-harmonic dynamics (top, black line); (ii) as the compression increases the system becomes bistable and can commute from one well to the other, greatly increasing $z_{r.m.s.}$ which reaches its maximum at $c \sim 1.5$ % (top, red line); (iii) larger compressions, $c > 1.5$ %, get the system trapped in one of the two wells, being the barrier high enough to prevent swings to the other one (top, blue line). Interestingly, the modulation of the 2D polarization P_x^{2D} keeps on increasing with the compression and is largest when the ribbons dynamics gets stuck in one of the wells of the bistable potential (Fig. ??, bottom). As previously reported [?], this happens because in this regime $\frac{\partial P_x^{2D}}{\partial Z}$ is much larger, and even small variations of the amplitude of the vibrating mode result in large changes in the polarization.

From the device design viewpoint it is important to choose the applied compressive strain c that maximizes the harvested power. Naively, one can assume that the optimal value of c is the one that maximizes $z_{r.m.s.}$. We have already shown that this is not necessarily the case [?] and that at large c larger variation of P_x^{2D} can compensate the reduction of $z_{r.m.s.}$, leading to a saturation of the r.m.s. of the power. In Fig. ?? we plot $z_{r.m.s.}$ and the r.m.s. of the piezovoltage, $V_{r.m.s.}$, as a function of c . The curves with the empty symbols have been calculated using the elastic energy obtained with the Tersoff potential plot-

ted in Fig. ?? and assuming a Langevin effective dynamics within that potential landscape. The results are qualitatively similar to those obtained with density-functional calculation in Ref. [?], with $z_{r.m.s.}$ exhibiting a peak at $c \sim 1.5\%$ and $V_{r.m.s.}$ saturating at 1.5 mV. The curves with the filled symbols, on the other hand, have been calculated directly from the MD simulation.

As one can see, the $z_{r.m.s.}$ is in good agreement with the one calculated from the effective dynamics, at least for what the thresholds of the different dynamical regimes are concerned. Due to the limitations of the model based on Langevin dynamics, on the other hand, non negligible differences emerge when looking at $V_{r.m.s.}$ (black circles). What happens is that, as compression increases, oscillations along x cannot be neglected. These oscillations, which yield vibrational modes that are no longer purely transverse and cannot be captured in the effective description of the Langevin dynamics (where the effective mass moves long z), are fully accounted for when P_x^{2D} is calculated from Eq. ?? throughout the MD run. This means that when using the same 2D material as mechanical and piezoelectric transducer, the more adapted working regime is the 11 (strain and polarization with parallel directions): out-of-plane oscillations induce both in-plane and out-of-plane strains generating a measurable voltage along the nanoribbon direction, x . A better agreement can be recovered by applying an external stochastic force in the MD simulations, forcing the atoms to move only along z (red diamonds).

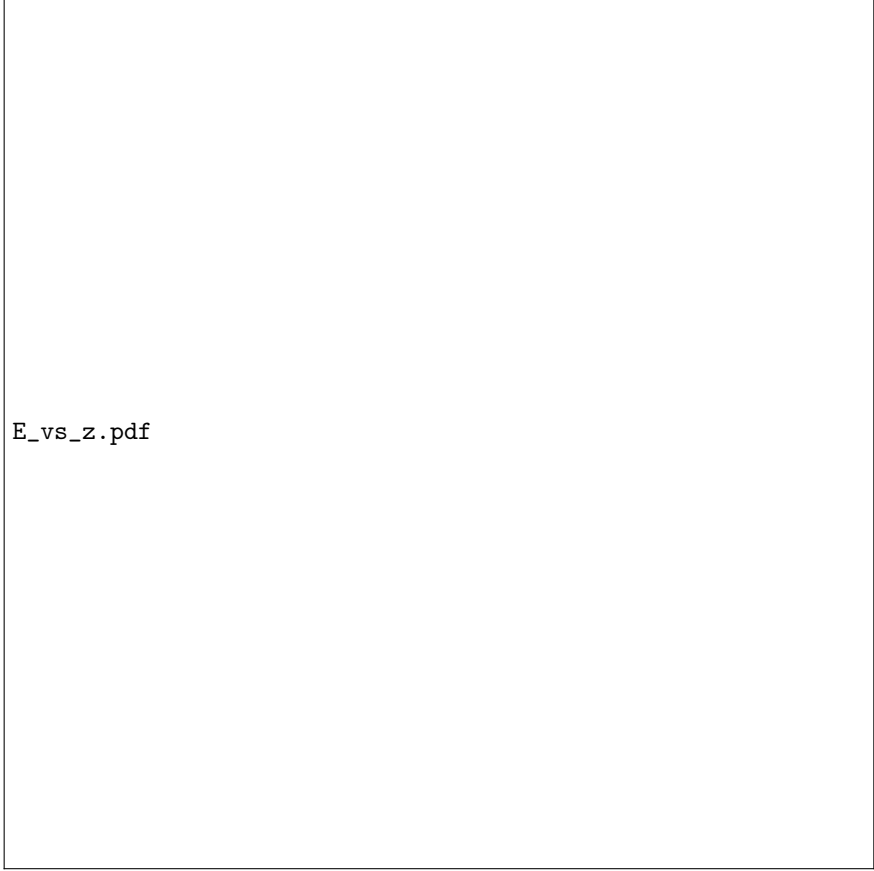
Conclusions

We have studied the dynamics of a h -BN armchair nanoribbon as a function of an applied compressive strain for energy harvesting applications. This is a simple and compact design for nanoscale ambient vibration harvesting, as the mechanical oscillator operates simultaneously as a piezoelectric transducer. These calculations go beyond the simplified description provided thus far in terms of an effective mass. Our calculations show that engineered nonlinearities greatly increase the device performances in term of harvested power.

Importantly, the unification of the mechanical and the electromechanical transducer elements in one single material structure not only simplifies a possible fabrication process, but also broadens the range of compression that increases the device performance.

structs.pdf

Figure 1: (a) Sketch of the three different dynamics regimes. Left: quasi-harmonic oscillation in the single-well potential; middle: double-well potential where oscillations in each well combine with stochastic low frequency swings from one well to the other; right: double-well potential where the barrier is too large to be overcome with a given level of ambient noise, E_{noise} . (b) Two- and four-atom unit cells of monolayer *h*-BN. (c) Buckled configuration of a compressed clamped-clamped BN nanoribbon.



E_vs_z.pdf

Figure 2: (a) Potential energy per BN pair of the $100.7 \text{ nm} \times 7.2 \text{ nm}$ h -BN as a function of the amplitude of the sinusoidal deformation for different values of the compressive strain ϵ . The inset shows the dependence of the depth of the well and distance between minima that appear for finite values of ϵ . (b,c) Comparison between the potential energy per BN pair as a function of the amplitude of the deformation obtained with the Tersoff potential used throughout this work and the DFT computational framework of Ref. [?]. The data of panels (b) and (c) refer to the structural model (the only one for which we could afford the computationally intensive DFT calculations) used in Ref. [?]: a $17 \text{ nm} \times 1 \text{ nm}$ supercell of 2D h -BN without edges.

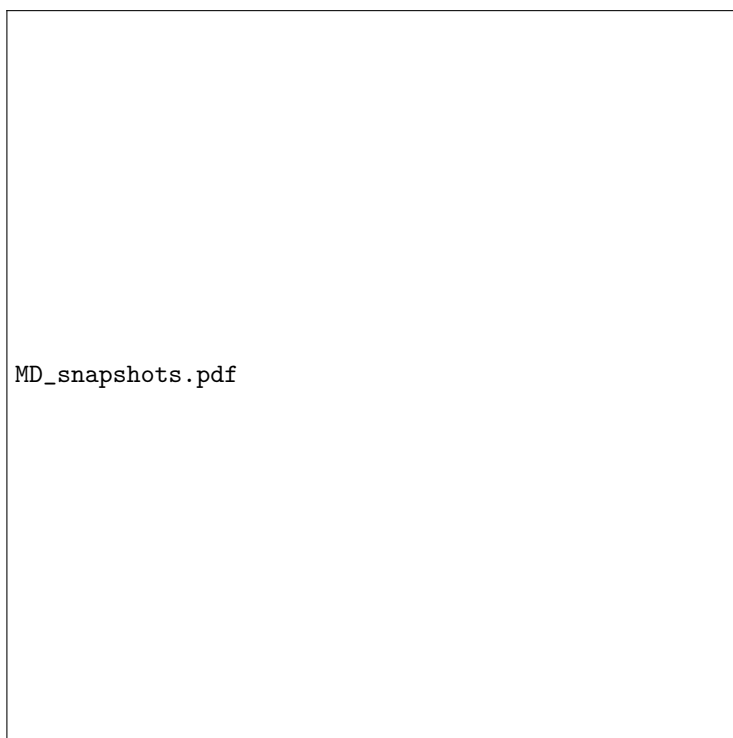


Figure 3: Snapshot of the dynamics of a BN nanoribbon subjected to a compression of 1.5 %.

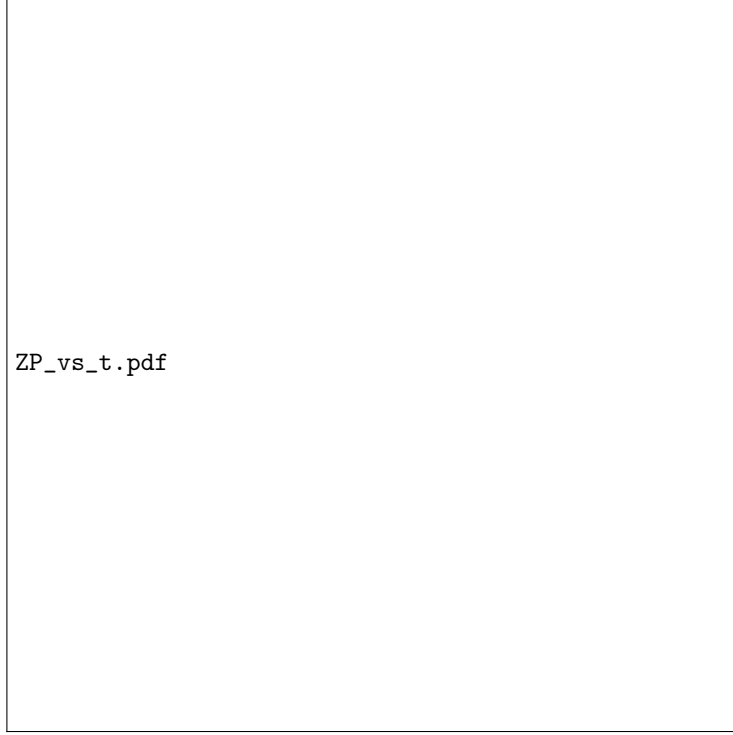


Figure 4: (Top) Dependence of $z_{r.m.s.}$ with time for three representative dynamics regimes in MD simulations with $T_{eff} = 120$ K and an external stochastic force along z : (i) no compression applied ($c = 0$ %); (ii) a finite compression drives the system to bistability ($c = 1$ %); (iii) large applied compression, the system gets stuck in one of the minima of the double-well potential ($c = 2.5$ %). (Bottom) Histogram of the polarization P_x^{2D} in the three cases of the top panel. The broadening of the curve with the increasing compression is the fingerprint of the enhanced piezoelectric response. These results correspond to an external stochastic force, F_{ext} ,

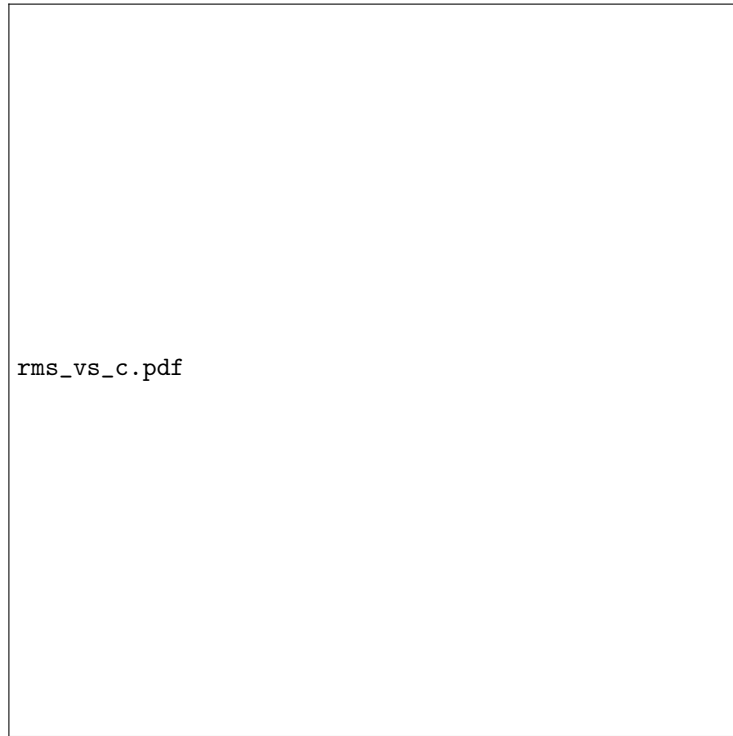


Figure 5: $z_{r.m.s.}$ and $V_{r.m.s.}$ as a function of the compression calculated within an effective Langevin dynamics (black circles) or from the full atomistic MD simulation (red diamonds).